Advanced characterization of circumferential and radial hydrides in reactor-grade Zirconium cladding tube to enhance the understanding of their precipitation mechanisms

Dahyeon Woo, Youho Lee*
Department of Nuclear Eng., Seoul National Univ., 1 Gwanak-ro Gwanak-gu, Seoul 08826, Republic of Korea
**Corresponding author: leeyouho@snu.ac.kr*

***Keywords : Dry storage, Hydride reorientation, EBSD, TEM, DSC**

1. Introduction

During dry storage, hydride reorientation occurs when cladding hoop stress exceeds the threshold stress. Since the through-wall cracking can easily occur with radial hydrides, hydride reorientation significantly degrades the cladding integrity [1]. Therefore, accurate modeling of hydride reorientation is important to understand the spent nuclear fuel cladding behavior. In hydride reorientation modeling, microstructure information of hydride and zirconium matrix is required. However, experimental difficulty in detecting reactor-grade Cold Work Stress Relieved (CWSR) Zirconium with Electron Backscatter Diffraction (EBSD) has hampered the direct observation of Zirconium hydrides. This study presents successful EBSD characterization of hydrided CWSR Zirconium. Additionally, Transmission Electron Microscope (TEM), and Differential Scanning Calorimetry (DSC) were conducted for microstructural characterization. Preferred sites of hydride precipitation, orientations for Zirconium matrix neighboring to hydrides, and interface in Zirconium hydrides according to the macroscopic orientation of hydrides were determined. And how it advances the current understanding and gross assumptions of microstructural characteristics of hydrided Zirconium will be discussed.

2. Experimental

2.1. Hydrogen charging and hydride reorientation

Unirradiated reactor-grade Zirconium cladding tube with an outer diameter of 9.5 mm and thickness of 0.57 mm was used in this study. Hydrogen was charged in cladding for ~200 wppm at 400 ℃.

Using hydrogen-charged cladding tubes, hydride reorientation was conducted via the pressurization method. After heating up to 400 ℃, the cladding was cooled down to room temperature with a cooling rate of 0.396 ℃/min. The maximum temperature of 400 ℃ complies with the regulatory limit of the U.S. Nuclear Regulatory Commission (U.S. NRC) for dry storage [2]. During the cooling process, the internal pressure was applied while the cladding outer pressure was maintained at 1 atm to apply hoop stress. A specimen with only circumferential hydrides and specimens with various amounts of radial hydrides were fabricated.

2.2. Microstructural characterization (EBSD, TEM, and DSC)

Circumferential hydrides precipitated under hoop stress of 0 MPa and radial hydrides EBSD precipitated under 87, 110, and 142 MPa were observed using EBSD. EBSD images were analyzed in the ring surface (RD-TD plane) using a field emission scanning electron microscope (JEOL JSM-7900F), EBSD (Oxford instruments Nanoanalysis Symmetry S2), and orientation imaging microscopy (OIM) analysis software.

And TEM (JEOL JEM-ARM200F) was used to determine the orientation relationship (OR) and interface. TEM lamellas were prepared with a focused ion beam (FEI, Helios 650) from the cladding tube surface.

For DSC analysis, 4 mm ring specimens were cut into 4 sub-specimens and mechanically polished to make the bottom surface flat. Using DSC (Netzsch STA 449 F5), each specimen was heated up to the target maximum temperature of 600 ℃ and cooled down to room temperature at a rate of 20 ℃/min. After DSC measurement, the hydrogen concentration was measured using ELTRA ONH-2000.

2.3. Construction of 3D Interface in EBSD

OR includes three degrees of freedom, which are the orientation of two crystals and their rotation angle. Therefore, OR determines the relative position of two crystals. However, two additional information are required to define the interface: the boundary trace angle on the surface and the boundary inclination angle along axial direction (Fig. 1(a)). The typical EBSD image which captures the ring surface includes 4 information (Fig. 1(b)). The only missing information is the boundary inclination angle. Due to the pilgering process during cladding fabrication, cladding tubes have axially parallel grains [3]. In this study, it was found that most inter-granular hydrides and even intra-granular hydrides precipitate along the axial direction in the Transmission Kikuchi Diffraction (TKD) image. Therefore, the interface between the hydride and Zr matrix was assumed to be parallel with the axial direction in EBSD interface characterization. Additionally, to determine the boundary trace angle, the phase boundaries in the EBSD image were reconstructed according to the macroscopic morphology of hydrides.

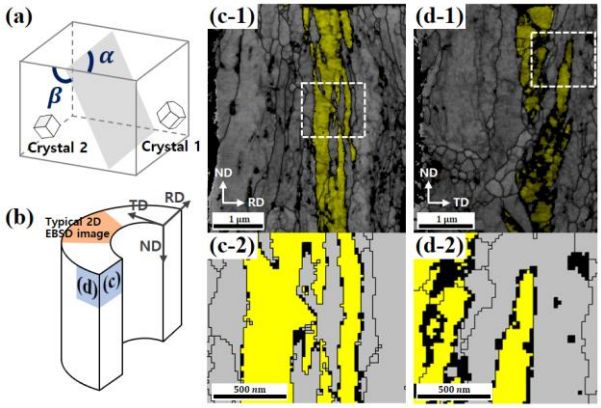

Fig. 1. (a) Schematic image of interface, (b) chematic image of cladding tube geometry, (c) TKD image of circumferential hydride, (d) TKD image of radial hydride.

3. Result and Discussion

3.1. Orientation relationship and interface analysis

OR between hydride and Zr matrix was determined in TEM. Total OR analysis results are presented in Table I. OR of (0001)//(111) [1$\bar{2}$10]//[110] was dominant both in circumferential and radial hydrides. Additionally, to evaluate OR in EBSD, the interplanar angle between the (0001) plane in α-Zr and (111) in δ-hydride was calculated in all interfaces. The interplanar angle of 0° indicates the parallel condition of the two planes. It was found that ~80% of the total interface lengths have interplanar angles below 10° in both circumferential hydrides and radial hydrides. OR was close to (0001)// (111) which shows consistent results with TEM.

Table I: OR analysis results in TEM

OR	0 MPa $\delta_{H,Cir}$	142 MPa $\delta_{H,Rad}$
(0001)//(111) [1$\bar{2}$10]//[110]	5	2
(0001)//(001) [1$\bar{2}$10]//[110]	-	1

Grain tilted angle from the radial direction was calculated in addition to the interface angle from the basal plane, to address the texture of Zirconium cladding. EBSD interface characterization results are presented in Fig. 2. In 0 MPa, most of the interfaces were placed in the circumferential direction. The interfaces were not in a specific angle combination and they took various angle combinations. Similarly, in 142 MPa radial hydrides, radial interfaces were dominant and they revealed various angle combinations.

Statistical EBSD analysis results show the difference between circumferential and radial hydrides in the orientation of α-Zr grains where hydrides precipitate. While both circumferential and radial hydrides exhibit a similar interface which is ~30° from the basal plane of HCP structure, circumferential hydrides and radial hydrides mostly precipitated at the α-Zr grain which have ~30° and ~60° tilted orientations from RD (Fig. 2(a-2), (b-2)). In the past understanding of circumferential and radial hydrides, the grain orientation angle was fixed at 0°, and the interface was considered to be different: the basal and prismatic plane [4]. However, in reactor-grade Zirconium cladding, it was found that hydride reorientation is the consequence of picking up different sites in terms of grain orientation.

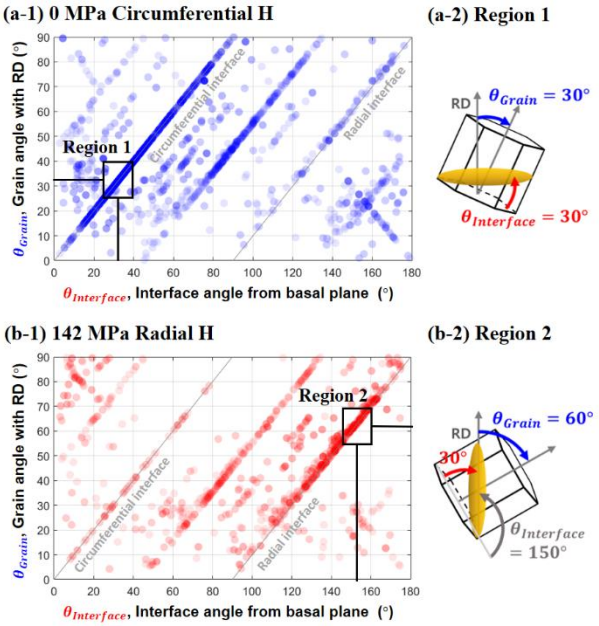

Fig. 2. (a-1), (b-1): Interface characterization in circumferential and radial hydrides, respectively. (a-2), (b-2): Schematic image for the peak region of Region 1 and Region 2, respectively.

In addition to the EBSD, interfaces were detected in TEM using the edge-on method as presented in Fig. 3. (10$\bar{1}$3)//(110) interface was detected in 0 MPa circumferential hydride (Fig. 3(a)), and (10$\bar{1}$0)//(110) interface was detected in 142 MPa radial hydride (Fig. 3(b)). Both EBSD and TEM show incoherent interfaces of hydride and reactor-grade Zr matrix in circumferential and radial hydrides.

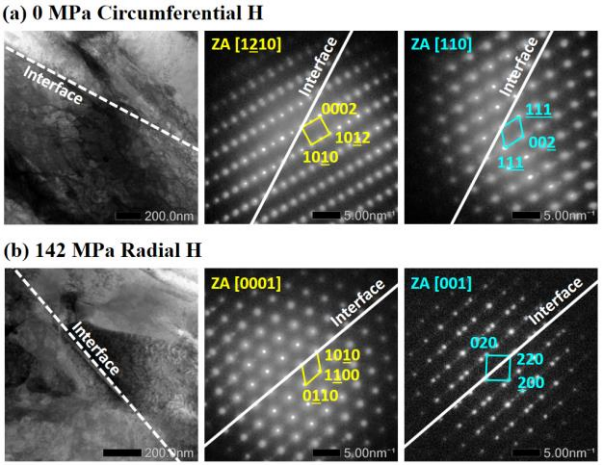

Fig. 3. TEM interface analysis results in (a) circumferential hydride, and (b) radial hydride.

In EBSD and TEM, it was found that there is no significance in interface energy between circumferential and radial hydrides. DSC analysis was conducted to investigate the solubility and dissolution energy of hydrides. In the DSC curve, the terminal solubility of dissolution (TSSD) temperature was determined as the maximum temperature of the peak region, and the dissolution energy was calculated by integrating the area under the peak region. The solubility curve with TSSD temperature from DSC and hydrogen concentration from OH-p is presented in Fig. 4(a). The two measurements made a good agreement with the theoretical TSSD curve [5]. In Fig. 4(a), there was no significant difference in solubility between circumferential and radial hydrides. The calculated dissolution analysis results are presented in Fig. 4(b). Dissolution energy linearly increased with hydrogen concentration and it was similar in circumferential and radial hydrides, which supports the observation from EBSD and TEM.

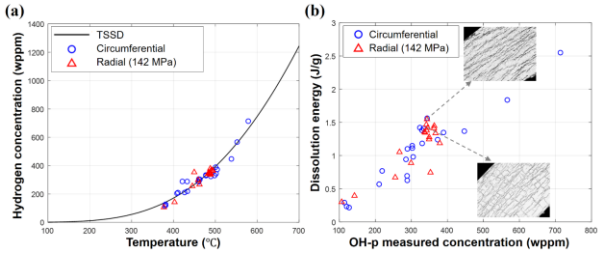

Fig. 4. (a) TSSD analysis result, (b) dissolution energy analysis result in circumferential and radial hydrides.

Incoherent interfaces were detected in EBSD and TEM interface analyses. For incoherent interfaces, the volume misfit strain dictates the total misfit strain [6]. Since the volume misfit strain basically arises from different packing density of Zr (HCP) and hydride (FCC), volume misfit strain would be similar in circumferential and radial hydrides (~17% [7]). This implies that the misfit strain remains similar level in circumferential and radial hydrides, and the subtle difference in strain energy might occur from the different shapes of circumferential and radial hydrides. This result revisits the need to correct the field's prevailing assumption that circumferential hydrides and Zr matrix form coherent interfaces of (0001)//(111) based on the characterization of non-reactor grade recrystallized Zr plate specimens.

3.2. Hydride precipitation mechanism depending on the stress state

According to the site of precipitation, hydrides are classified into three types: inter-granular hydride, intra-granular hydride, and trans-granular hydride. If the intra-granular hydrides keep growing and cut across the grain, it is intra-granular hydride. Three types of hydrides in circumferential and radial hydrides are presented in Fig. 5. The crystallographic orientation of Zr grains which are placed on both sides of blue-colored trans-granular grains are exactly same. In 0 MPa, intra-granular hydrides appeared at the tip of interconnected inter-granular hydrides. Significant amount of trans-granular hydride appeared in radial hydrides of 142 MPa.

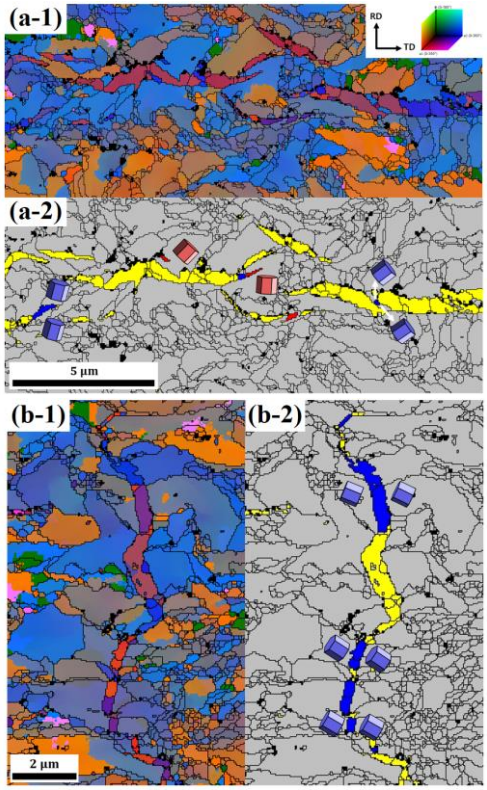

Fig. 5. EBSD Euler map and phase map of (a) 0 MPa circumferential hydride, (b) 142 MPa radial hydride. (In the phase map, yellow color indicates inter-granular hydride, red color indicates intra-granular hydride, and blue color indicates trans-granular hydride)

The fraction of three types of hydrides in circumferential and radial hydrides is presented in Fig. 6. Consistent with the general understanding that hydrides prefer to precipitate at the grain boundary, inter-granular hydride was dominant in circumferential hydride, reaching ~90%. However, the fraction of inter-granular hydrides in radial hydrides remained at only ~65% and the fraction of intra/trans-granular hydrides increased up to ~35%.

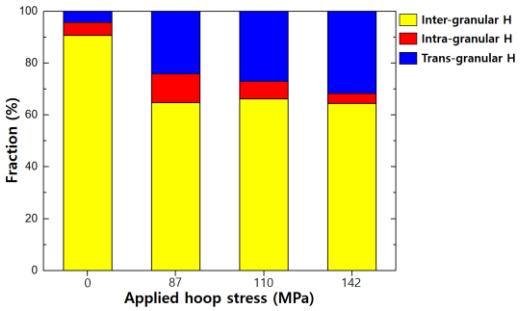

Fig. 6. Fraction of three types of hydrides in 0 MPa circumferential hydrides and radial hydrdies precipitated under 87, 110, and 142 MPa.

The orientations of Zr grains with each hydride type are presented in Fig. 7. It was found that circumferential hydrides pick up the statistically favorable grains, which are tilted 30° from the radial direction (Fig. 7(a)). In radial hydrides, Zr grains with inter-granular exhibited similar behavior with circumferential hydrides (Fig. 7(b-1)). However, intra/trans-granular hydrides favored 60° tilted Zr grains even with the limited number of available sites, due to the applied stress (Fig. 7(b-2)).

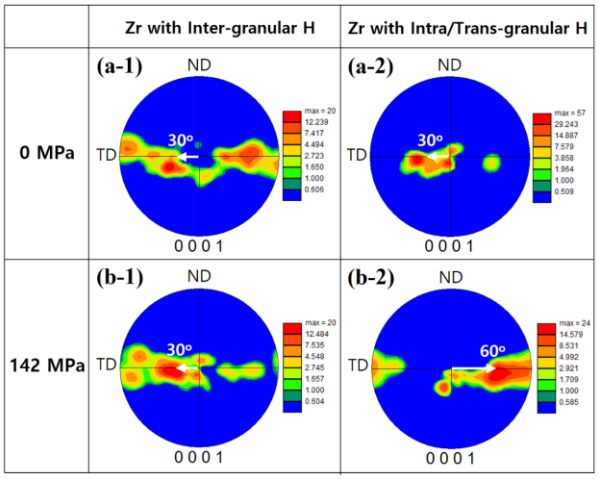

Fig. 7. Pole figures of Zr grains neighboring to (a-1) inter-granular H in 0 MPa, (a-1) intra/trans-granular H in 0 MPa, (b-1) inter-granular H in 142 MPa, (b-2) intra/trans-granular Hin 142 MPa.

Reactor-grade Zirconium cladding tubes have a circumferentially elongated grain structure. Therefore, without stress, circumferential hydrides precipitate at the circumferential grain boundaries which serve as the dominant nucleation site (Fig. 8(a-1)). Once hydride is precipitated along circumferential grain boundary, hydride growth occurs near the pre-existing hydride tip due to the low chemical potential resulting from misfit stress. In circumferentially elongated grain structure, the connectivity of circumferential grain boundary is high, such that additional hydrides grow along the circumferential grain (Fig. 8(a-2)).

Applied hoop stress increases the local strain in radial grain boundaries such that radial grain boundary energy is get raised. Therefore, earlier radial hydrides precipitate in radial grain boundaries perpendicular to hoop stress (Fig. 8(b-1)). And due to the effect of lowered chemical potential near hydride tip, hydride growth occurs. However, due to the low connectivity of radial grain boundaries, hydrides precipitate as intra/trans-granular hydrides ((Fig. 8(b-2)) which were found with a high fraction in Fig. 6.

The evidence of an earlier stage of radial hydride was found in the specimen with apparently short radial hydride in 29.7 wppm and 133 MPa case. As can be seen in Fig. 9, radial hydride consists of inter-granular hydrides. Additionally, in this study, all the intra and trans-granular hydrides were precipitated together with inter-granular hydrides. Therefore, radial hydride first precipitates at the radial grain boundary which is perpendicular to the hoop stress, and the low radial boundary connectivity resulted in the growth of a fraction of intra/trans granular hydrides.

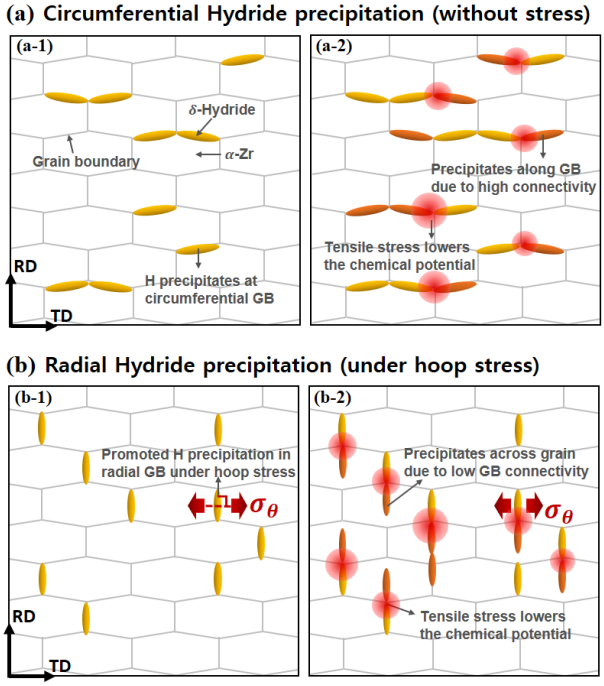

Fig. 8. Schematic image of precipitation mechanism of hydrides (a) without hoop stress, (b) under hoop stress.

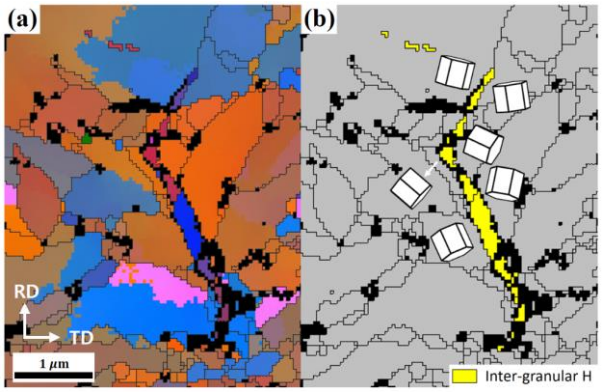

Fig. 9. EBSD (a) Euler map and (b) phase map radial hydride only with inter-granular hydrides

4. Conclusion

Zirconium hydrides in the CWSR Zirconium cladding tube were successfully characterized using EBSD. Interface analysis results in EBSD and TEM show incoherent interfaces between hydride and Zr matrix in both circumferential and radial hydrides. Considering the most probable interfaces, it was found that the interface planes in HCP crystal were similar in circumferential and radial hydrides (~30° from the basal plane) and they picked up Zr grains with different orientations (~30°

from RD in circumferential hydrides and ~60° from RD in radial hydrides). These results imply the need to introduce the frame of volume misfit strain rather than the lattice misfit strain for hydride reorientation modeling.

It was found that circumferential hydrides precipitate at circumferential grain boundaries which are predominant sites in circumferentially elongated Zr grain structure. Additional hydride precipitation occurred along circumferential grain boundaries due to their high connectivity. Under hoop stress, hydrides precipitate at radial grain boundaries whose hydrogen potency increased due to applied stress. Additional hydride precipitation occurs across the grain due to the low connectivity of radial hydrides, which results in the generation of intra/trans-granular hydrides.

Some macroscopic properties in grain level and microstructural characterization in radial hydrides precipitated under various stresses (87 MPa, 110 MPa) will be additionally discussed.

ACKNOWLEDGEMENT

This work was supported by the Nuclear Safety Research Program through the institute for Korea Spent Nuclear Fuel (iKSNF) using the financial resource granted by the Ministry of Science and ICT (MSIT) of the Republic of Korea [No. 2021M2E1A108598612].

REFERENCES

[1] D. Woo, Y. Lee, Understanding the mechanical integrity of Zircaloy cladding with various radial and circumferential hydride morphologies via image analysis, Journal of Nuclear Materials 584 (2023) 154560.
[2] U.S. NRC, Spent Fuel Project Office Interim Staff Guidance-11, Revision 3.
[3] W. Qin, J.A. Szpunar, J. Kozinski, Hydride-induced degradation of hoop ductility in textured zirconium-alloy tubes: A theoretical analysis, Acta Mater. 60 (2012) 4845–4855.
[4] S. Kim, JH. Kang, Y. Lee, Suppressed hydride precipitation in the welding zone of a zirconium-based alloy cladding tube, Journal of Nuclear Materials 580 (2023) 154406.
[5] G. Sabol, G. Moan, Zirconium in the nuclear industry: twelfth international symposium, (2000).
[6] DAVID A. POTER, Phase Transformations in Metals and Alloys, CRC Press.
[7] BRIAN W. LEITCH, MANFRED P. PULS, Finite Element Calculations of the Accommodation Energy of a Misfitting Precipitate in an Elastic-Plastic Matrix, Met. Trans. A, 23A (1992), p. 797.